

PACS numbers: 81.05.uf; 79.20.Eb
DOI: 10.1070/QE2015v045n05ABEH015759

Negative pressure and spallation in graphite targets under nano- and picosecond laser irradiation

R.S. Belikov, I.K. Krasyuk, T. Rienecker, A.Yu. Semenov, O.N. Rosmej, I.A. Stuchebryukhov, M. Tomut, K.V. Khishchenko, A. Schoenlein

Abstract. **We present the results of experiments on the spallation phenomena in graphite targets under shock-wave nano- and picosecond irradiation, which have been performed on Kamerton-T (GPI, Moscow, Russia) and PHELIX (GSI, Darmstadt, Germany) laser facilities. In the range of the strain rates of 10^6–10^7 s^{-1}, the data on the dynamic mechanical strength of the material at rapure (spallation) have been for the first time obtained. With a maximal strain rate of 1.4×10^7 s^{-1}, the spall strength of 2.1 GPa is obtained, which constitutes 64% of the theoretical ultimate tensile strength of graphite. The effect of spallation is observed not only on the rear side of the target, but also on its irradiated (front) surface. With the use of optical and scanning electron microscopes, the morphology of the front and rear surfaces of the targets is studied. By means of Raman scattering of light, the graphite structure both on the target front surface under laser exposure and on its rear side in the spall zone is investigated. A comparison of the dynamic strength of graphite and synthetic diamond is performed.**

Keywords: *laser radiation of picosecond and nanosecond duration, ablation pressure, shock wave, negative pressure, spallation phenomenon, strain rate, ultimate strength, numerical simulation, graphite.*

1. Introduction

This paper presents the results of experiments on studying the spallation phenomenon in graphite targets. To produce a tensile stress (negative pressure), the samples were subjected to the shock-wave action of laser pulses with duration of 1.4 ns on the PHELIX laser system (GSI, Darmstadt, Germany) and of 70 ps on the Kamerton-T laser system (GPI, Moscow, Russia). In both cases, the laser wavelength was 0.53 μm.

The phenomenon of spallation is used to obtain the knowledge on the dynamic tensile strength of a material [1]. Spallation occurs near the rear (free) surface of the target as a result of reflection of the compression wave generated by the action of a laser radiation pulse on the front side of a target. As a result of reflection, a free surface of the target comes into motion, thus causing the unloading wave propagation towards the compression pulse (which is also succeeded by the wave of unloading). At some distance from the rear surface of the target the pressure becomes negative (herewith, the tension may exceed the tensile strength of the material) and a spall layer is formed, which comes off from the original target.

In the experiments, the samples of MF-307 (with the density of 2 g cm^{-3}) and PG (with the density of 1.84 g cm^{-3}) polycrystalline graphite were investigated.

The upper estimate for theoretical ultimate tensile strength σ_t of a substance can be derived, based on the parameters of its shock adiabat, from the formula $\sigma_t = \rho c_0^2/(4b)$, where ρ is the substance density; c_0 and b are the coefficients of the shock adiabat $D = c_0 + bU$ [2]; D is the shock wave velocity; and U is the mass velocity. For MF-307 graphite, from the database of shock-wave experiments [3] we have $c_0 = 3$ km s^{-1} and $b = 1.35$. As a result, we obtain the upper estimate of 3.3 GPa for the tensile strength of MF-307 graphite. A similar value in the case of PG graphite turns out equal to 2.7 GPa.

The interest in studying the dynamic mechanical strength of graphite is due to the fact that, to date, there is no published data on the physical properties of graphite at negative pressures. It is also interesting to compare the data on the dynamic strength of graphite with similar data on another allotropic form of carbon, i.e. that of diamond.

2. Experimental conditions

The experiments were performed using Kamerton-T and PHELIX neodymium glass laser systems. The laser radiation of these systems was converted into the second harmonic with a wavelength of 0.53 μm. The laser pulse energy in the first case was 1 J, while in the second it was 120 J. The laser beam was focused on the target into a spot with a diameter of 0.4 to 3.7 mm. The maximum flux density of laser radiation in the focusing region reached 1.6×10^{13} W cm^{-2}, with the ablation pressure equal to 0.6 TPa. The data of these experiments are given in Table 1. Figure 1 shows the transverse distribution of laser radiation in the near zone (Kamerton-T) and the X-ray pinhole picture of the hot zone in the focal region (PHELIX). A scheme of the experiments is shown in Fig. 2.

The morphology of the front and rear surfaces of the samples after laser irradiation was investigated by a scanning electron microscope (SEM). The destruction zone and the crater depth on both sides of the samples were measured using

I.K. Krasyuk, A.Yu. Semenov, I.A. Stuchebryukhov A.M. Prokhorov General Physics Institute, Russian Academy of Sciences, ul. Vavilova 38, 119991 Moscow, Russia, e-mail: krasyuk@kapella.gpi.ru;
R.S. Belikov, K.V. Khishchenko Joint Institute for High Temperatures, Russian Academy of Sciences, ul. Izhorskaya 13, Bld. 2, 125412 Moscow, Russia;
O.N. Rosmej GSI Helmholtzzentrum für Schwerionenforschung GmbH, Planckstraße 1, 64291 Darmstadt, Germany;
T. Rienecker, A. Schoenlein Goethe University Frankfurt am Main, Grüneburgplatz 1, 60323 Germany;
M.Tomut Technische Universität Darmstadt, Karolinenplatz 5, 64289 Darmstadt, Germany

Received 29 January 2015; revision received 10 April 2015
Kvantovaya Elektronika **45** (5) 421–425 (2015)
Translated by M.A. Monastyrskiy

Table 1. Experimental data.

Sample No.	Sample	D_{inp}/mm	E_{las}/J	I_{las}/TW cm^{-2}	p_a/Mbar	D_{sp}/mm	H_0/μm	h_{sp}/μm
1	MF-307 graphite	0.343	0.748	11.0	4.1	0.343	220	65
2	(Camertone-T, τ = 70 ps,	0.370	0.941	11.5	4.3	0.411	220	70
3	λ = 0.53 μm)	0.288	0.826	16.0	5.5	0.320	410	175
4	PG-5 graphite	3.70	122	2.1	1.3	3.1	2100	400
5	(PHELIX, τ = 1.4 ns,	1.35	120	6.0	2.8	3.5	2000	200
6	λ = 0.53 μm)	1.35	107	5.4	2.6	2.87	1100	80

Notes: D_{inp} is the focal spot diameter; E_{las} is the laser pulse energy; I_{las} is the laser radiation intensity in the focal spot on the target; p_a is the ablative pressure; D_{sp} is the spall zone diameter; H_0 is the target thickness; h_{sp} is the spall plate thickness; and τ and λ are the duration and wavelength of the laser radiation, respectively.

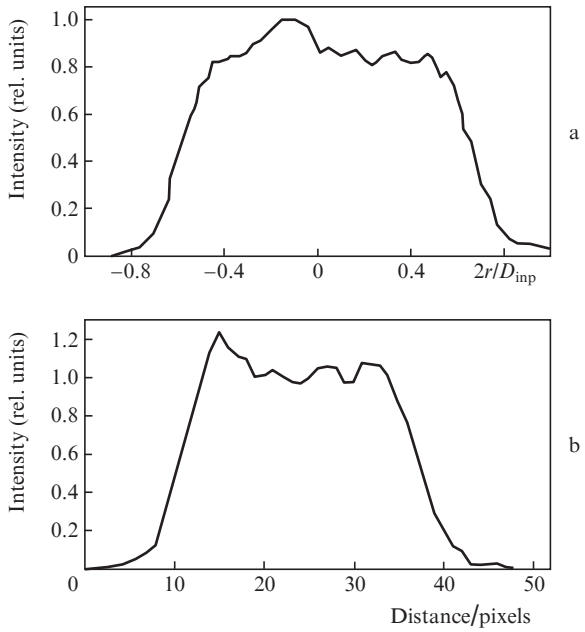

Figure 1. (a) Transverse distribution of laser radiation in the Kamerton-T facility in the near zone and (b) the X-ray pinhole picture of the hot zone in the focus region on the target for the PHELIX facility; 1 pixel is equal to 50 μm, and the hot area size is 1.35 μm.

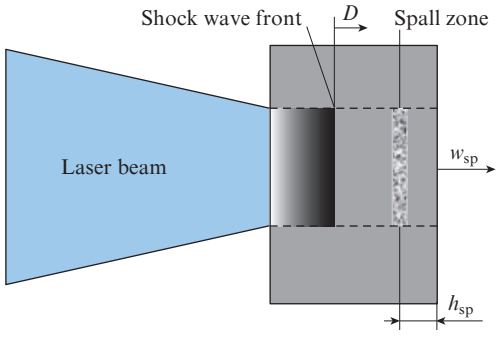

Figure 2. Scheme of the experiments (D is the velocity of the shock wave front; and h_{sp} and w_{sp} are the thickness and velocity of the spall plate, respectively).

an optical MF-8 metallographic microscope with an accuracy of 1 μm.

The substance structure on the irradiated and the spall surfaces of the target was analysed by the method of Raman scattering of light using the confocal HR800-180 spectrometer (Horiba Jobin Yvon) with a spectral resolution of 0.5 cm^{-1}. For Raman scattering excitation, two types of lasers were used: a He–Ne-laser with a wavelength λ = 632.8 nm (20 mW power) and an Nd:YAG-laser with λ = 532 nm (40 mW power). In both cases, the spatial resolution was 2 μm.

3. A method of determining the spall strength and strain rate

To determine the spall strength σ^* and the strain rate $\dot{V}/V_0$ of a substance (V_0 is initial specific volume and $\dot{V}$ is its change rate), we have used an approach based on the measurement of the spall recess depth h_{sp} after the pulse laser action on a target, with subsequent mathematical modelling of the shock-wave process in the sample [4, 5]. To calculate the values σ^* and $\dot{V}/V_0$, a numerical code was used, which implements the Courant–Isaacson–Rice algorithm on the basis of the hydrodynamic equations [6]. This code uses the equation of state for graphite, obtained from the semi-empirical model [7]. It is assumed that the pulse shape of ablative pressure on the target front surface follows the laser pulse shape.

The relationship between the pulse amplitude of ablative pressure p_a (in TPa) and the laser radiation intensity I_{las} (in TW cm^{-2}) was defined by the semi-empirical formulas [8]

$$p_a = \begin{cases} 1.2(10^{-2} I_{las})^{2/3} \lambda^{-2/3} [A/(2Z)]^{3/16} \text{ at } I_{las} \geqslant 4.3 \text{ TW cm}^{-2}, \\ 1.4(10^{-2} I_{las})^{7/9} \lambda^{-3/4} \text{ at } I_{las} < 4.3 \text{ TW cm}^{-2}, \end{cases}$$

where λ is the laser radiation wavelength in μm; A is the atomic weight; and Z is the atomic number of the target material.

In the experiments, the laser pulse intensity at which the spallation occurs was registered. After that, a numerical simulation of the shock wave propagation in the target was carried out. The results of one of the variants of calculations are shown in Fig. 3. In that case, the spall strength (the tensile strength) at the threshold amplitudes of the shock impact was defined as a modulus of the minimal calculated pressure (negative in magnitude) in the spall plane: $\sigma^* = |p_{min}|$ (Fig. 3c). The strain rate was determined from the calculated dependence $\rho(t)$ of the density on time (Fig. 3d) by means of its differentiation with respect to time: $\dot{V}/V_0 = |\dot{\rho}(t)/\rho_0|$.

4. Results

4.1. Morphology of the spall surface of targets

The top of Fig. 4 shows the SEM-images of the rear (spall) side of sample 1 after the shock-wave action, obtained with

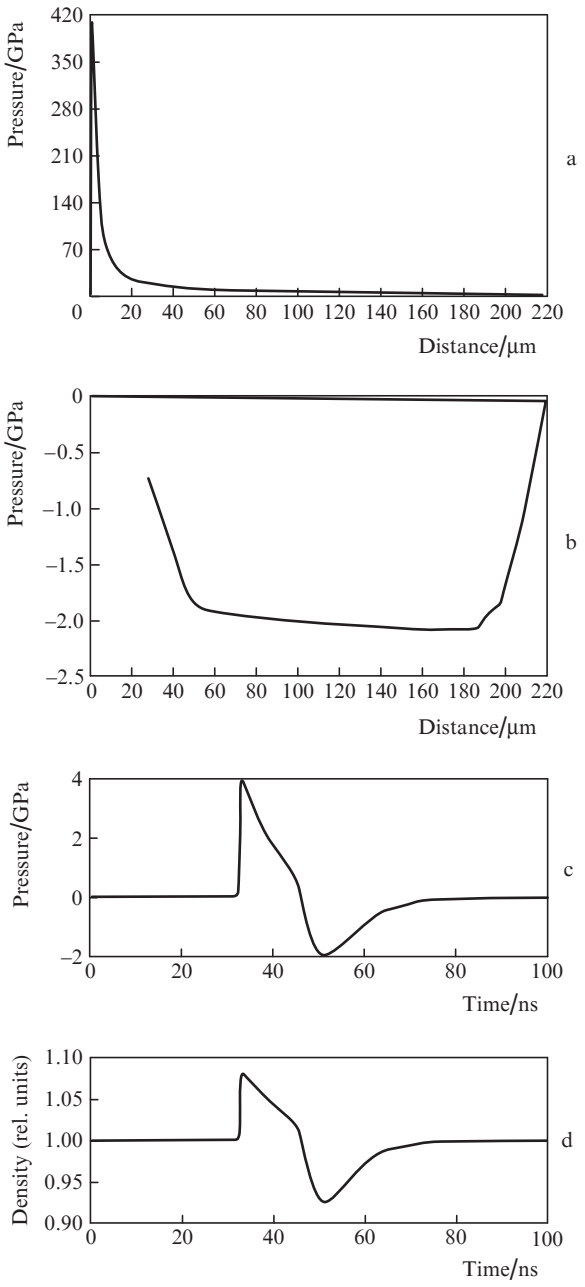

Figure 3. Results of calculations according to experiment 1: the distribution through the target thickness of (a) the maximal and (b) minimal pressure magnitudes, as well as evolution in time of (c) the pressure and (d) compression ratio (relative density) in the spall plane.

various magnifications. A spall occurred in experiment 6; herewith, the spall plate has not separated from the target, thus having been preserved for a further analysis. The optical image of this plate is shown at the bottom of Fig. 4. The plate has a quasi-conical shape, with an apex angle of 120°. This considerably differs from the case of metals, where the spall plates are of flat shape [9].

4.2. Structure of graphite on front and rear sides of the target

The main crystalline phase of MF-307 graphite (samples 1–3) is the graphite having a hexagonal crystal structure. This

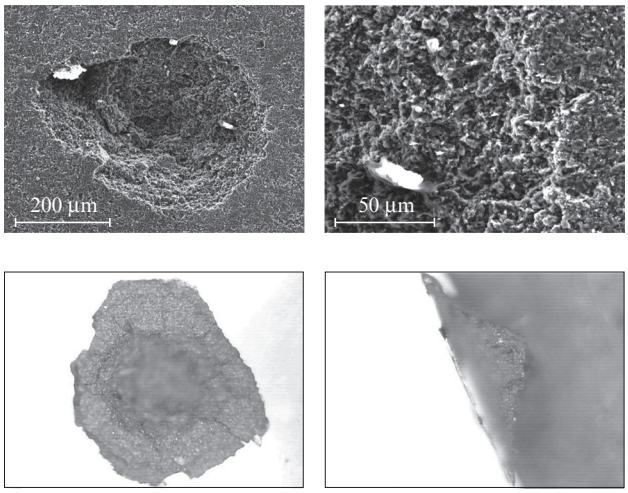

Figure 4. SEM images with different magnification of the rear (spall) side of sample 1 after the shock-wave action (top) and also the optical image of the inner side (left) and from the end-face (right) of the spall plate preserved in experiment 6 (the angle at the top of the spall plate is 120°).

material, along with crystalline phases, comprises a small portion of amorphous component. The samples of PG-5 graphite (samples 4–6) represent the polycrystalline graphite with the grains that have a size of ~20 nm.

The results of Raman spectroscopy of samples 4 and 5 of PG-5 graphite after laser irradiation are shown in Fig. 5 and Table 2.

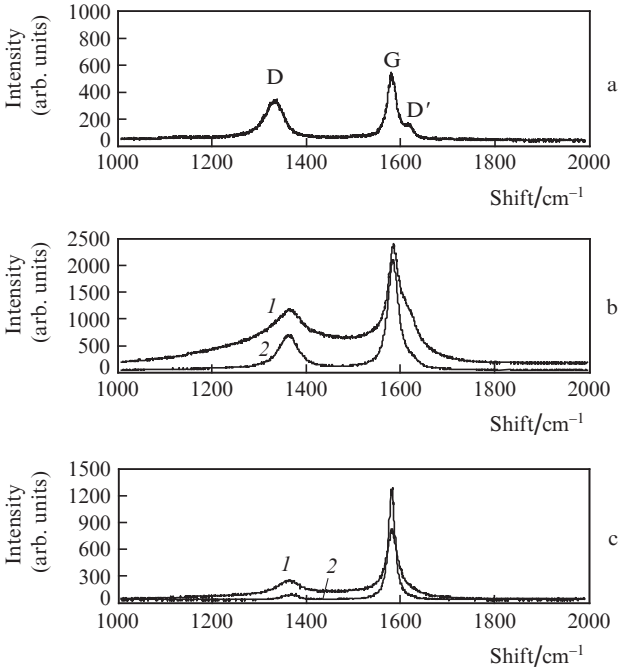

Figure 5. Raman spectra for a PG-5 target: (a) outside the laser exposure area, (b) in experiment 4 on the front surface of the target in the laser exposure area at the edge (*1*) and at the centre (*2*) of the impact zone, (c) in experiment 5 in the laser exposure area on the front surface of the target (*1*) and in the zone of spall crater on the rear surface of the target (*2*).

Table 2. Characteristics of lines of Raman spectra of PG-5 graphite samples.

Sample	I_D/I_G	Δ_G/cm^{-1}	Δ_D/cm^{-1}
Initial	0.59	24.5	47.8
4 (laser exposure area, crater edge)	0.42	51.4	100
4 (laser exposure area, crater centre)	0.31	27.7	51.1
5 (laser exposure area, crater centre)	0.25	32.1	89.9
5 (spall crater zone)	0.12	21.4	50

Notes: I_D/I_G is the ratio of intensities of the spectral lines D and G; and Δ_G and Δ_D are the widths of the lines D and G at the half-height.

Figure 5a shows the Raman spectrum of the initial sample of PG-5 graphite. Here, the Raman G-line corresponds to the Raman line position in monocrystalline graphite, while the Raman D-line appears due to the finite size of crystallites, as well as due to the disorder and possible defects in the sample, the Raman D′-line usually accompanies the appearance of the line D.

Figure 5b shows the Raman spectra obtained in the region of laser action on the front surface of the target in the course of experiment 4. Curve (*2*) corresponds to the crater centre, curve (*1*) – to its edge. Analysis of these spectra allows the following conclusions. In the crater centre, the material represents the graphite with a perfect structure resulting from the recrystallization of the original material. At the crater edge, the substance most probably possesses a disordered graphite structure, which is characteristic of the turbostratic form of carbon being close to the structure of carbon black.

Figure 5c represents the Raman spectra registered in the course of experiment 5 in the region of laser action on the front surface of the target [curve (*1*)] and in the area of the spall crater on the rear surface of the target [curve (*2*)]. The Raman spectrum in the spall area indicates a well-recrystallized structure of graphite, with a small disorder and a greater degree of crystallinity compared to the original material.

4.3. Dependence of the spall strength of graphite samples on the strain rate

Figure 6 shows the dependence of the graphite spall strength σ^* on the strain rate $\dot{V}/V_0$. Using the method of least squares, the data are approximated by the curve described by the expression $\sigma^* = 6.7\times10^{-2}(\dot{V}/V_0)^{0.36}$. The inaccuracies in determining the spall strength σ^* and the strain rate $\dot{V}/V_0$ are mainly caused by a finite width of the spall zone. The analysis of experimental data and results of calculations show that the maximum errors in determining the spall strength and strain rate are 5% and 38%, respectively. The experiments give the spall strength $\sigma^* \approx 2.1$ GPa, which constitutes 64% of the theoretical tensile strength 3.27 GPa for graphite, calculated according to the equation of state [7].

Figure 7 presents the data on the dynamic strength of synthetic diamond and graphite [10]. It can be seen that, with the strain rate of 10^7 s^{-1}, the spall strengths of graphite and diamond may presumably coincide. However, this requires additional measurement of the diamond's spall strength at the strain rates of $(1–1.2)\times10^7$ s^{-1}.

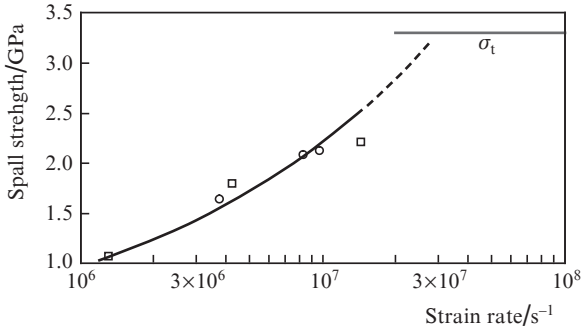

Figure 6. Dependence of the spall strength of graphite on the strain rate measured on the Kamerton-T (○) and PHELIX (□) facilities.

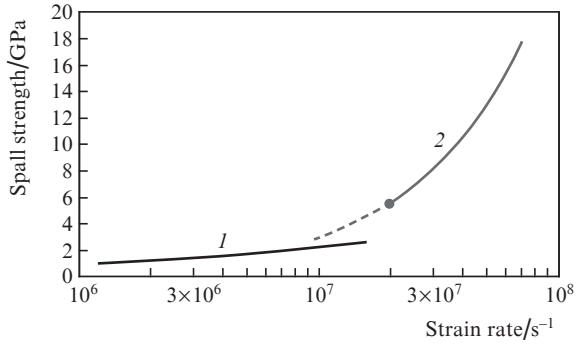

Figure 7. Dynamic strength of (*1*) graphite and (*2*) synthetic diamond [10]. The dashed line represents a continuation of the experimental curve (*2*) into the region of strain rates that lie below the range (●) studied in [10].

5. Conclusions

The main result of this research is that the data on the dynamic strength of graphite at the strain rates of $10^6–10^7$ s^{-1} have been for the first time obtained. The maximal spall strength of $\sigma^* \approx 2.1$ GPa reached in the experiments constitutes 64% of the theoretical tensile strength of the material. The Raman spectra obtained are indicative of the changes in the crystalline structure of graphite compared to its original state, both on the front surface of the target in the area of laser exposure and on its rear side in the spall zone.

Acknowledgements. The authors express their gratitude to A.I. Savvatimskii for providing the samples of MF-307 graphite, as well as to R.O. Gavrilin, S.M. Savin, A.V. Bogdanov, V.A. Panyushkin, A.V. Bakhmutova, A.P. Kuznetsov and K.L. Gubskiy for their help in the experiments.

This work was supported by the Russian Foundation for Basic Research (Grant Nos 12-02-00625, 12-02-00746, 13-02-91057, 14-08-00967 and 14-29-06099), the RF President's Grants Council (State Support to the Leading Scientific Schools Programme, Grant Nos NSh-451.2014.2 and NSh-6614.2014.2) and the Presidium of the Russian Academy of Sciences (Extreme Light Fields and Their Applications Programme No. 13P; and Matter at High Energy Densities Programme No. 2P). We are grateful for the support offered by programme FP7 EuCARD-2 (Grant No. 312453) and by the Federal Ministry of Education and Research (BMBF) of Germany.

References

1. Zeldovich Ya.B., Raiser Yu.P. *Physics of Shock Waves and High-Temperature Hydrodynamic Phenomena* (New York: Acad. Press, 1966; Moscow: Fizmatlit, 2008).
2. Kanel' G.I., Razorenov S.V., Utkin A.V., Fortov V.E. *Shock-Wave Phenomena and the Properties of Condensed Matter* (New York: Springer, 2004; Moscow: Janus-K, 1996).
3. Levashov P.R., Khishchenko K.V., Lomonosov I.V., Fortov V.E. *Proc. Conf. Shock Compression of Condensed Matter-2003* (Melville, NY, AIP, 2004) p. 87; http://www.ihed.ras.ru/rusbank/, http://www.ficp.ac.ru/rusbank/.
4. McQueen R.G., March D. *J. Appl. Phys.*, **33** (2), 654 (1962).
5. Batani D., Vovchenko V.I., Kanel' G.I., et al. *Dokl. Ross. Akad. Nauk*, **389** (3), 328 (2003).
6. Kulikovskii A.G., Pogorelov N.V., Semenov A.Yu. *Matematicheskie voprosy chislennogo resheniya giperbolicheskikh system* (Mathematical Problems of Numerical Solution of The Hyperbolic Equation Systems) (Moscow: Fizmatlit, 2012) p. 608.
7. Lomonosov I.V., Fortov V.E., Khishchenko K.V. *Khim. Fiz.*, **14** (1), 47 (1995).
8. Vovchenko V.I., Krasyuk I.K., Pashinin P.P., Semenov A.Yu. *Dokl. Ross. Akad. Nauk*, **338** (3), 322 (1994).
9. Abrosimov S.A., Bazhulin A.P., Voronov V.V., et al. *Kvantovaya Elektron.*, **43** (3), 246 (2013) [*Quantum Electronics*, **43** (3), 246 (2013)].
10. Abrosimov S.A., Bazhulin A.P., Bolshakov A.P., et al. *Kvantovaya Elektron.*, **44** (6), 530 (2014) [*Quantum Electronics*, **44** (6), 530 (2014)].